Cell Reports, Volume *39*

Supplemental information

Altered BAF occupancy and transcription factor dynamics in PBAF-deficient melanoma

Saul Carcamo, Christie B. Nguyen, Elena Grossi, Dan Filipescu, Aktan Alpsoy, Alisha Dhiman, Dan Sun, Sonali Narang, Jochen Imig, Tiphaine C. Martin, Ramon Parsons, Iannis Aifantis, Aristotelis Tsirigos, Julio A. Aguirre-Ghiso, Emily C. Dykhuizen, Dan Hasson, and Emily Bernstein

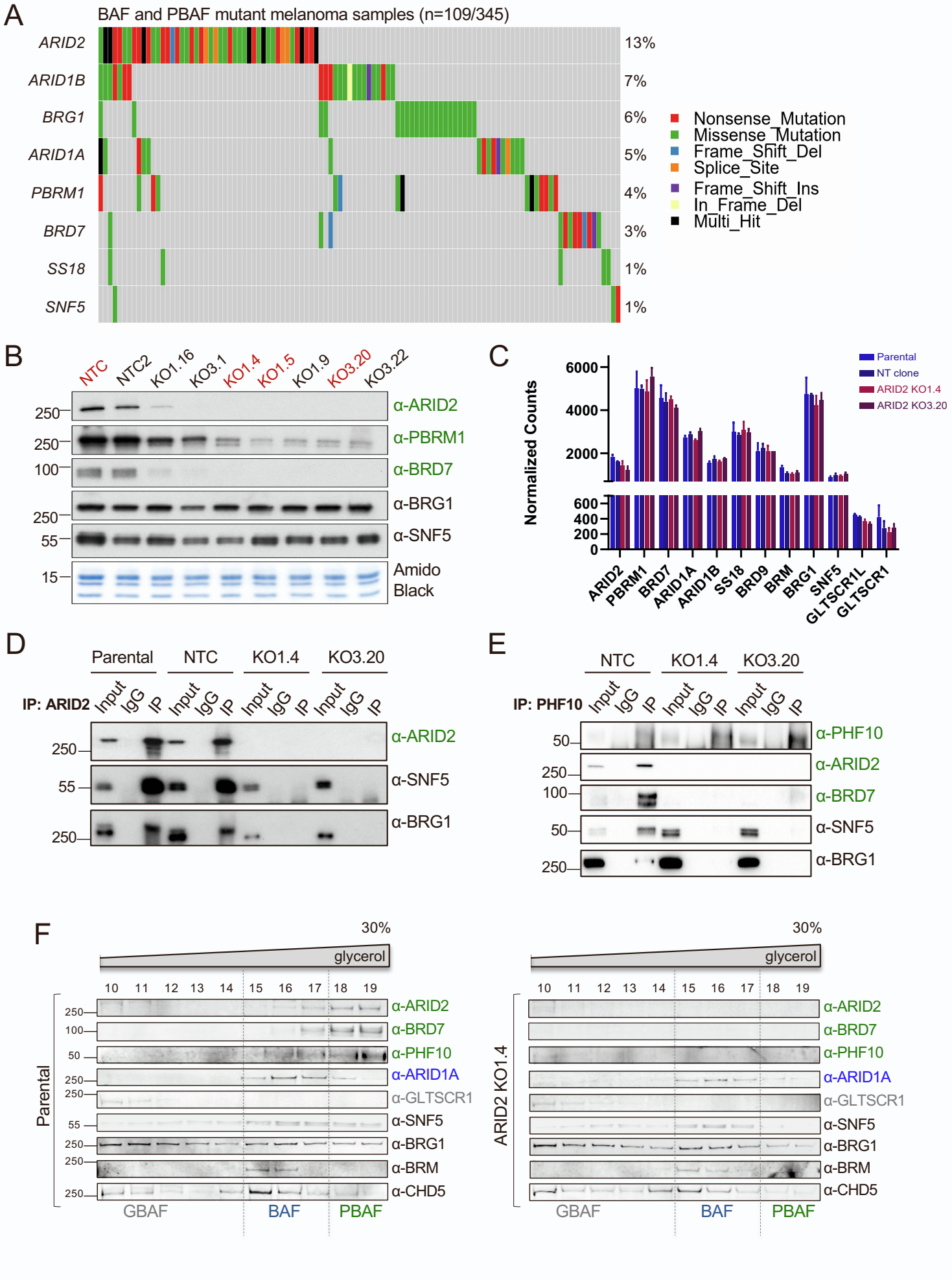
A
BAF and PBAF mutant melanoma samples (n=109/345)
ARID2
ARID1B
BRG1
ARID1A
PBRM1
BRD7
SS18
SNF5
13%
7%
6%
5%
4%
3%
1%
1%
Nonsense_Mutation
Missense_Mutation
Frame_Shift_Del
Splice_Site
Frame_Shift_Ins
In_Frame_Del
Multi_Hit
B
NTC
NTC2
KO1.16
KO3.1
KO1.4
KO1.5
KO1.9
KO3.20
KO3.22
α-ARID2
α-PBRM1
α-BRD7
α-BRG1
α-SNF5
Amido Black
C
Normalized Counts
Parental
NT clone
ARID2 KO1.4
ARID2 KO3.20
ARID2
PBRM1
BRD7
ARID1A
ARID1B
SS18
BRD9
BRM
BRG1
SNF5
GLTSCR1L
GLTSCR1
D
Parental
NTC
KO1.4
KO3.20
IP: ARID2
Input
IgG
IP
α-ARID2
α-SNF5
α-BRG1
E
NTC
KO1.4
KO3.20
IP: PHF10
α-PHF10
α-ARID2
α-BRD7
α-SNF5
α-BRG1
F
30%
glycerol
10 11 12 13 14 15 16 17 18 19
Parental
ARID2 KO1.4
α-ARID2
α-BRD7
α-PHF10
α-ARID1A
α-GLTSCR1
α-SNF5
α-BRG1
α-BRM
α-CHD5
GBAF
BAF
PBAF

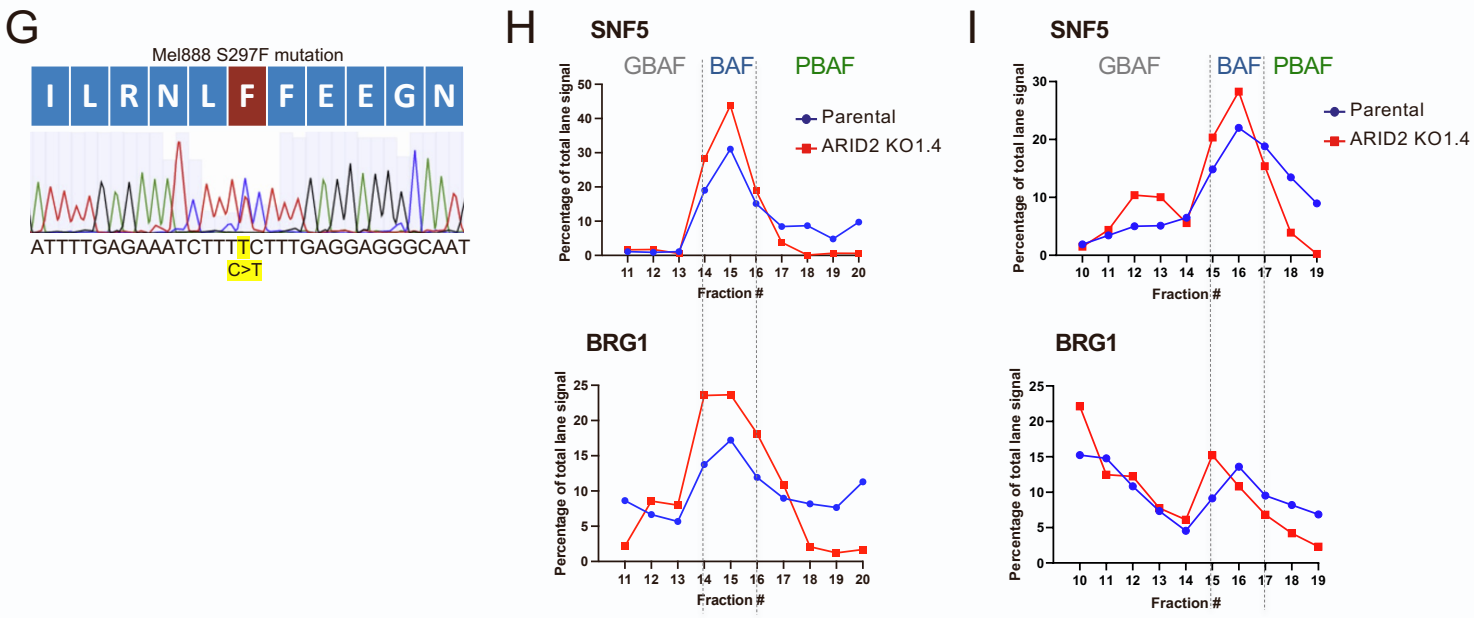

Figure S1. Effects of ARID2 loss on SWI/SNF complexes in melanoma, Related to Figure 1. A. Expanded oncoplot generated from The Cancer Genome Atlas' (TCGA) skin cutaneous melanoma (SKCM) mutational data set, highlighting some of the most commonly mutated SWI/SNF subunits across cancers. Columns represent samples. **B.** Chromatin fraction immunoblot of multiple SKmel147 ARID2 CRISPR clones. Blots were stained for PBAF-specific subunits ARID2, PBRM1 and BRD7 (green) and core subunits SNF5 and BRG1 (black). Amido black staining was used as loading control. Clones highlighted in red were used for further analysis. **C.** DEseq2 normalized counts (median of ratios) of multiple SWI/SNF subunits in SKmel147 ARID2 WT and ARID2 KO clones. **D.** Immunoblots of ARID2, SNF5 and BRG1 in SKmel147 ARID2 WT and KO cells following immunoprecipitation (IP) of endogenous ARID2 and IgG as negative control. **E.** Immunoblots of PHF10, ARID2, BRD7, SNF5 and BRG1 in SKmel147 ARID2 WT and KO cells following IP of endogenous PHF10 and IgG as negative control. **F.** Immunoblots of replicate glycerol gradient sedimentation from SKmel147 ARID2 WT and KO1.4. **G.** Sanger sequencing of Mel888 confirms ARID2 mutation (S297F). **H&I.** Quantification of glycerol gradient sedimentation immunoblots from **Figure 1E** and (**F**) respectively, for SNF5 and BRG1. ImageJ was used to calculate the staining intensity as area under the curve. The total signal was calculated (i.e. the total sum of the signals from each fraction per blot) to estimate the proportion of percent signal from each fraction.

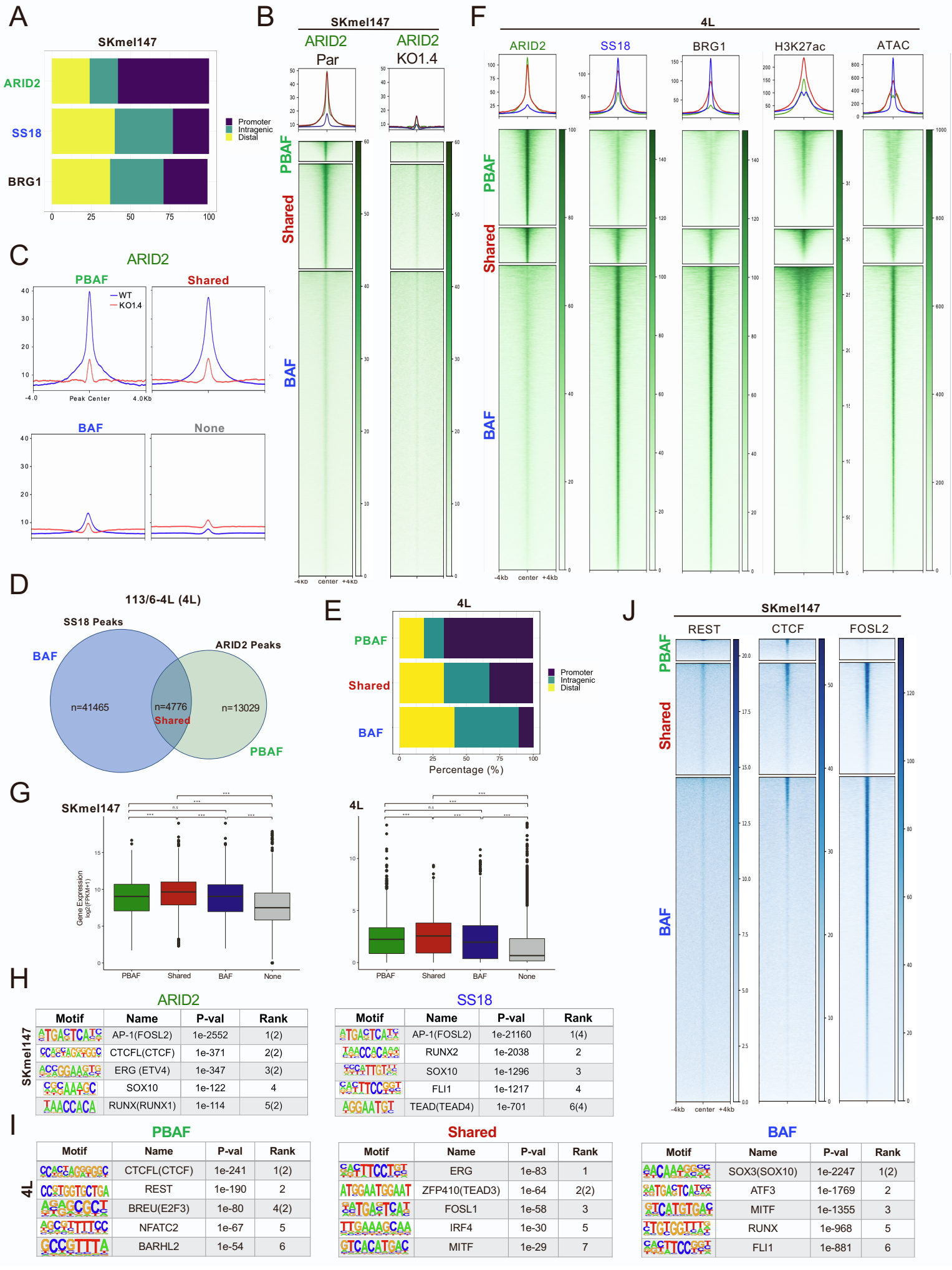
A
SKmel147
ARID2
SS18
BRG1
Promoter
Intragenic
Distal
0
25
50
75
100
B
SKmel147
ARID2
Par
ARID2
KO1.4
PBAF
Shared
BAF
-4kb
center
+4kb
C
ARID2
PBAF
Shared
WT
KO1.4
-4.0
Peak Center
4.0Kb
BAF
None
D
113/6-4L (4L)
SS18 Peaks
ARID2 Peaks
BAF
n=41465
n=4776
Shared
n=13029
PBAF
E
4L
PBAF
Shared
BAF
Promoter
Intragenic
Distal
Percentage (%)
F
4L
ARID2
SS18
BRG1
H3K27ac
ATAC
PBAF
Shared
BAF
-4kb
center
+4kb
G
SKmel147
4L
Gene Expression
log2(FPKM+1)
PBAF
Shared
BAF
None
J
SKmel147
REST
CTCF
FOSL2
PBAF
Shared
BAF
-4kb
center
+4kb
H
SKmel147
ARID2
Motif
Name
P-val
Rank
AP-1(FOSL2)
1e-2552
1(2)
CTCFL(CTCF)
1e-371
2(2)
ERG (ETV4)
1e-347
3(2)
SOX10
1e-122
4
RUNX(RUNX1)
1e-114
5(2)
SS18
Motif
Name
P-val
Rank
AP-1(FOSL2)
1e-21160
1(4)
RUNX2
1e-2038
2
SOX10
1e-1296
3
FLI1
1e-1217
4
TEAD(TEAD4)
1e-701
6(4)
I
4L
PBAF
Motif
Name
P-val
Rank
CTCFL(CTCF)
1e-241
1(2)
REST
1e-190
2
BREU(E2F3)
1e-80
4(2)
NFATC2
1e-67
5
BARHL2
1e-54
6
Shared
Motif
Name
P-val
Rank
ERG
1e-83
1
ZFP410(TEAD3)
1e-64
2(2)
FOSL1
1e-58
3
IRF4
1e-30
5
MITF
1e-29
7
BAF
Motif
Name
P-val
Rank
SOX3(SOX10)
1e-2247
1(2)
ATF3
1e-1769
2
MITF
1e-1355
3
RUNX
1e-968
5
FLI1
1e-881
6

Figure S2. Differential and shared genomic localization of ARID2 and SS18, Related to Figure 2. A. Bar plots displaying the percentage of ARID2, SS18, and BRG1 peaks in SKmel147 occupying promoters, distal and intragenic regions mapped using clusterProfiler. **B.** Heatmaps of ChIP-seq enrichments of ARID2 in SKmel147 ARID2 WT (Parental) and KO (KO1.4) cells. Enrichment centered on PBAF, shared and BAF regions as defined by ARID2 and SS18 ChIP-seq significant peaks. Signals were plotted ± 4 kb around the peak centers. **C.** Metagene profiles of SKmel147 ARID2 WT (Parental) and KO (KO1.4) enrichment of ARID2 ChIP-seq, same as in (B), at PBAF, shared, and BAF regions, and at open chromatin regions detected by ATAC-seq that do not overlap with a PBAF, shared or BAF region (None). **D.** Intersection of significant peaks between ARID2 and SS18 ChIP-seq in 113/6-4L (4L) used to defined PBAF, BAF, and shared regions. **E.** Bar plots displaying the percentage of PBAF, shared, and BAF regions in 4L occupying promoters, distal, and intragenic regions mapped using clusterProfiler. Promoters (± 2 kb relative to TSS), intragenic and distal annotations were defined according to human hg19 gene annotation. **F.** Heatmaps of ChIP-seq enrichment for ARID2, SS18, BRG1, H3K27ac, and ATAC-seq centered on PBAF, shared, and BAF regions defined in (D). Signals were plotted ± 4 kb around the peak center. **G.** Box plots displaying gene expression of promoters in SKmel147 (left) and 4L (right) that intersect with a PBAF (n=1,721 and n=7,774), respectively), shared (n=8,833 and n=1,602), BAF region (n=3,790 and n=3,701), or none (n=3,646 and n=11,857) of those three regions. Significance calculated using ANOVA with Tukey's multiple comparison tests **H.** Transcription factor motif analysis of the ARID2 and SS18 regions centered at the summits of the ATAC peaks (± 200 bp) in Skmel147; generated with the HOMER suite. **I.** Transcription factor motif analysis of the PBAF, shared, and BAF regions centered at the summits of the ATAC peaks peaks (± 200 bp) in 4L; generated with the HOMER suite. **J.** Heatmaps of ChIP-seq enrichment for REST, FOSL2, and CTCF in SKmel147 cells centered on PBAF, shared, and BAF regions. Signals were plotted ± 4 kb around the peak center.

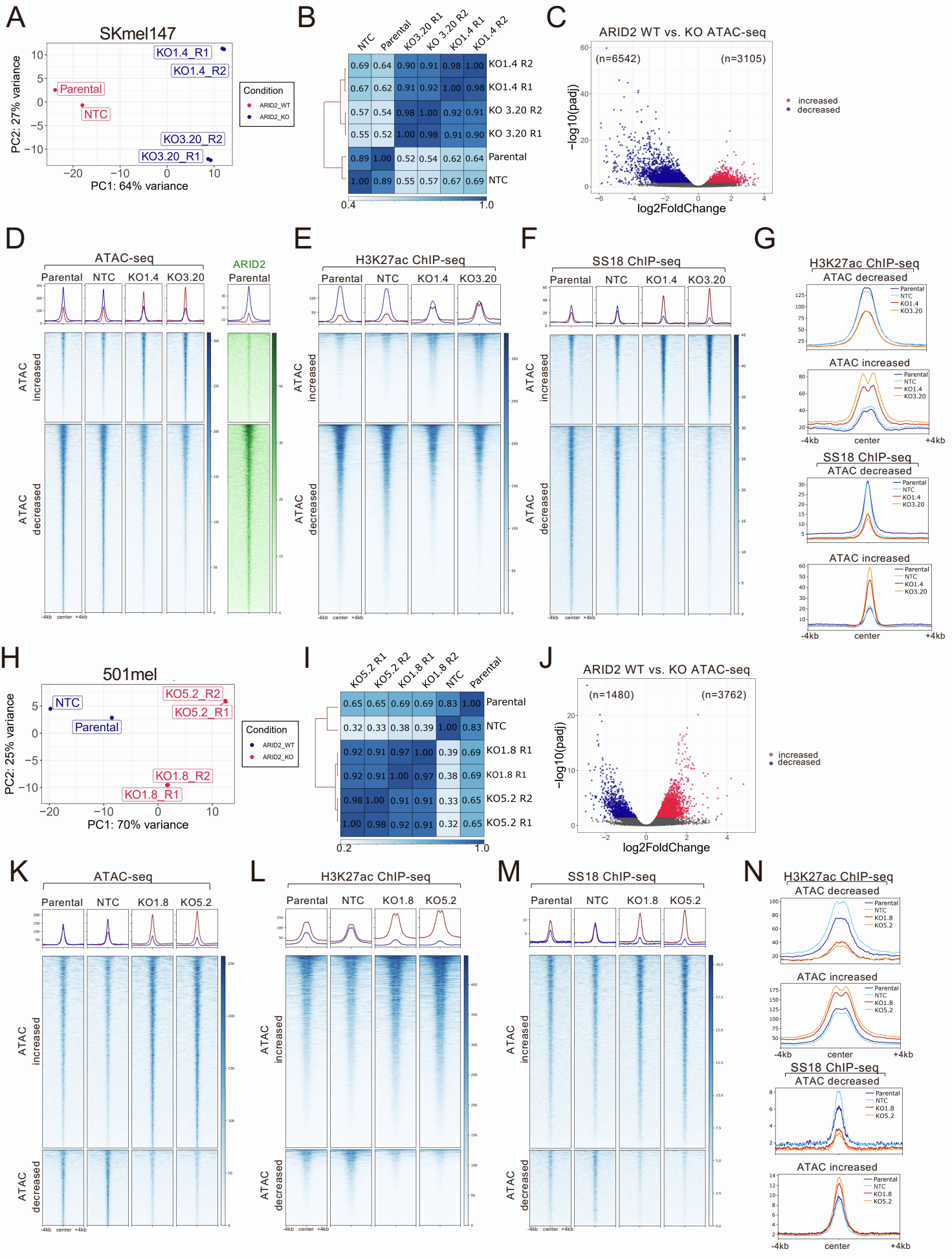
A
SKmel147
KO1.4_R1
KO1.4_R2
Parental
NTC
KO3.20_R2
KO3.20_R1
PC2: 27% variance
PC1: 64% variance
Condition
ARID2_WT
ARID2_KO
B
NTC
Parental
KO3.20 R1
KO 3.20 R2
KO1.4 R1
KO1.4 R2
KO1.4 R2
KO1.4 R1
KO 3.20 R2
KO 3.20 R1
Parental
NTC
C
ARID2 WT vs. KO ATAC-seq
(n=6542)
(n=3105)
−log10(padj)
log2FoldChange
increased
decreased
D
ATAC-seq
Parental
NTC
KO1.4
KO3.20
ARID2
Parental
ATAC increased
ATAC decreased
E
H3K27ac ChIP-seq
Parental
NTC
KO1.4
KO3.20
ATAC increased
ATAC decreased
F
SS18 ChIP-seq
Parental
NTC
KO1.4
KO3.20
ATAC increased
ATAC decreased
G
H3K27ac ChIP-seq
ATAC decreased
ATAC increased
SS18 ChIP-seq
ATAC decreased
ATAC increased
Parental
NTC
KO1.4
KO3.20
-4kb
center
+4kb
H
501mel
NTC
Parental
KO5.2_R2
KO5.2_R1
KO1.8_R2
KO1.8_R1
PC2: 25% variance
PC1: 70% variance
Condition
ARID2_WT
ARID2_KO
I
KO5.2 R1
KO5.2 R2
KO1.8 R1
KO1.8 R2
NTC
Parental
Parental
NTC
KO1.8 R1
KO1.8 R1
KO5.2 R2
KO5.2 R1
J
ARID2 WT vs. KO ATAC-seq
(n=1480)
(n=3762)
−log10(padj)
log2FoldChange
increased
decreased
K
ATAC-seq
Parental
NTC
KO1.8
KO5.2
ATAC increased
ATAC decreased
L
H3K27ac ChIP-seq
Parental
NTC
KO1.8
KO5.2
ATAC increased
ATAC decreased
M
SS18 ChIP-seq
Parental
NTC
KO1.8
KO5.2
ATAC increased
ATAC decreased
N
H3K27ac ChIP-seq
ATAC decreased
ATAC increased
SS18 ChIP-seq
ATAC decreased
ATAC increased
Parental
NTC
KO1.8
KO5.2
-4kb
center
+4kb

O

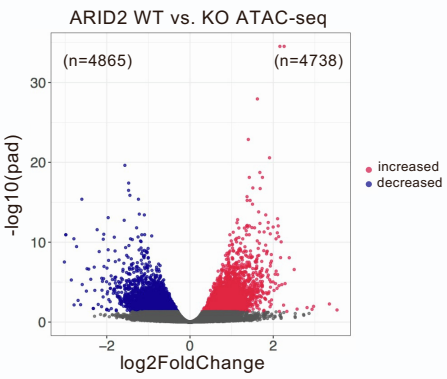
ARID2 WT vs. KO ATAC-seq
(n=4865)
(n=4738)
-log10(pad)
log2FoldChange
increased
decreased

P

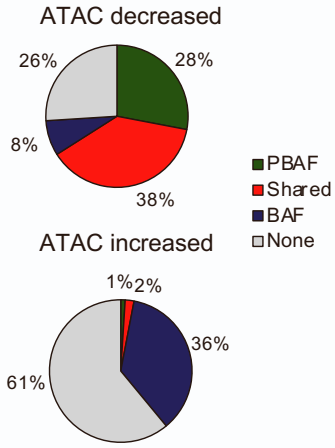
ATAC decreased
26%
28%
8%
38%
ATAC increased
1%
2%
36%
61%
PBAF
Shared
BAF
None

Q

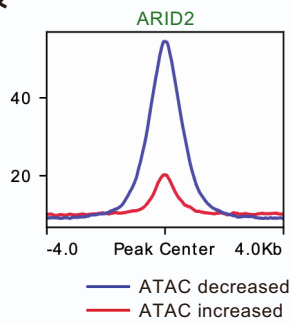
ARID2
40
20
-4.0
Peak Center
4.0Kb
ATAC decreased
ATAC increased

Figure S3. PBAF loss results in chromatin accessibility deregulation and altered BAF binding, Related to Figure 3. A. Two-dimensional PCA using all ATAC-seq significant regions (n=224,847) in SKmel147. **B.** Pearson correlation plot of the deregulated ATAC-seq regions in SKmel147. **C.** Volcano plot highlighting significantly increased (n = 6542) and decreased (n = 3105) ATAC-seq regions in SKmel147; called with DEseq2 with an adjusted p-value < 0.05. **D.** Heatmaps and metagene profiles of ATAC enrichment in SKmel147 ARID2 WT (Parental and NTC) and KO (KO1.4 and KO3.20) cells centered at ATAC-seq significantly deregulated regions; heatmap and metagene profile of ARID2 enrichment in ARID2 WT (Parental) cells shown. Signals were plotted ± 4 kb around the peak center. ATAC increased n = 3105 peaks, ATAC decreased n = 6542. **E.** Heatmaps and metagene profiles of H3K27ac enrichment as in (D), centered at ATAC-seq significantly deregulated regions. **F.** Heatmaps and metagene profiles of SS18 enrichment as in (D), centered at ATAC-seq significantly deregulated regions. **G.** Metagene profiles of H3K27ac and SS18 enrichment in SKmel147 ARID2 WT (Parental and NTC) and KO (KO1.4 and KO3.20) cells centered at ATAC-seq significantly deregulated regions. **H.** Two-dimensional PCA using all ATAC-seq significant regions (n=224,847) in 501mel. **I.** Pearson correlation plot of the differential ATAC-seq regions clustered by ARID2 status in 501mel. **J.** Volcano plot highlighting significantly increased (n = 3762) and decreased (n = 1480) ATAC-seq regions in 501mel; called with DEseq2 with an adjusted p-value < 0.05. **K.** Heatmaps and metagene profiles of ATAC enrichment in 501mel ARID2 WT (Parental and NTC) and KO (KO1.8 and KO5.2) cells centered at ATAC-seq significantly deregulated regions. Signals were plotted ± 4 kb around the peak center. ATAC increased n = 3762 peaks, ATAC decreased n = 1480. **L.** Heatmaps and metagene profiles of H3K27ac enrichment as in (K) centered at ATAC-seq significantly deregulated regions. **M.** Heatmaps and metagene profiles of SS18 as in (K) centered at ATAC-seq significantly deregulated regions. **N.** Metagene profiles of H3K27ac and SS18 enrichment in 501mel ARID2 WT (Parental and NTC) and KO (KO1.8 and KO5.2) cells centered at ATAC-seq significantly altered regions. **O.** Volcano plot highlighting significantly increased (n = 4738) and decreased (n = 4965) ATAC-seq regions in 4L; called with DEseq2 with an adjusted p-value < 0.05. **P.** Pie charts displaying the percentage of ATAC decreased and ATAC increased regions at PBAF, shared, and BAF sites, or None (no SWI/SNF binding). **Q.** Metagene profiles of ARID2 enrichment in 4L ARID2 WT (Parental) cells centered at ATAC-seq significantly deregulated regions. Signals were plotted ± 4 kb around the peak center.

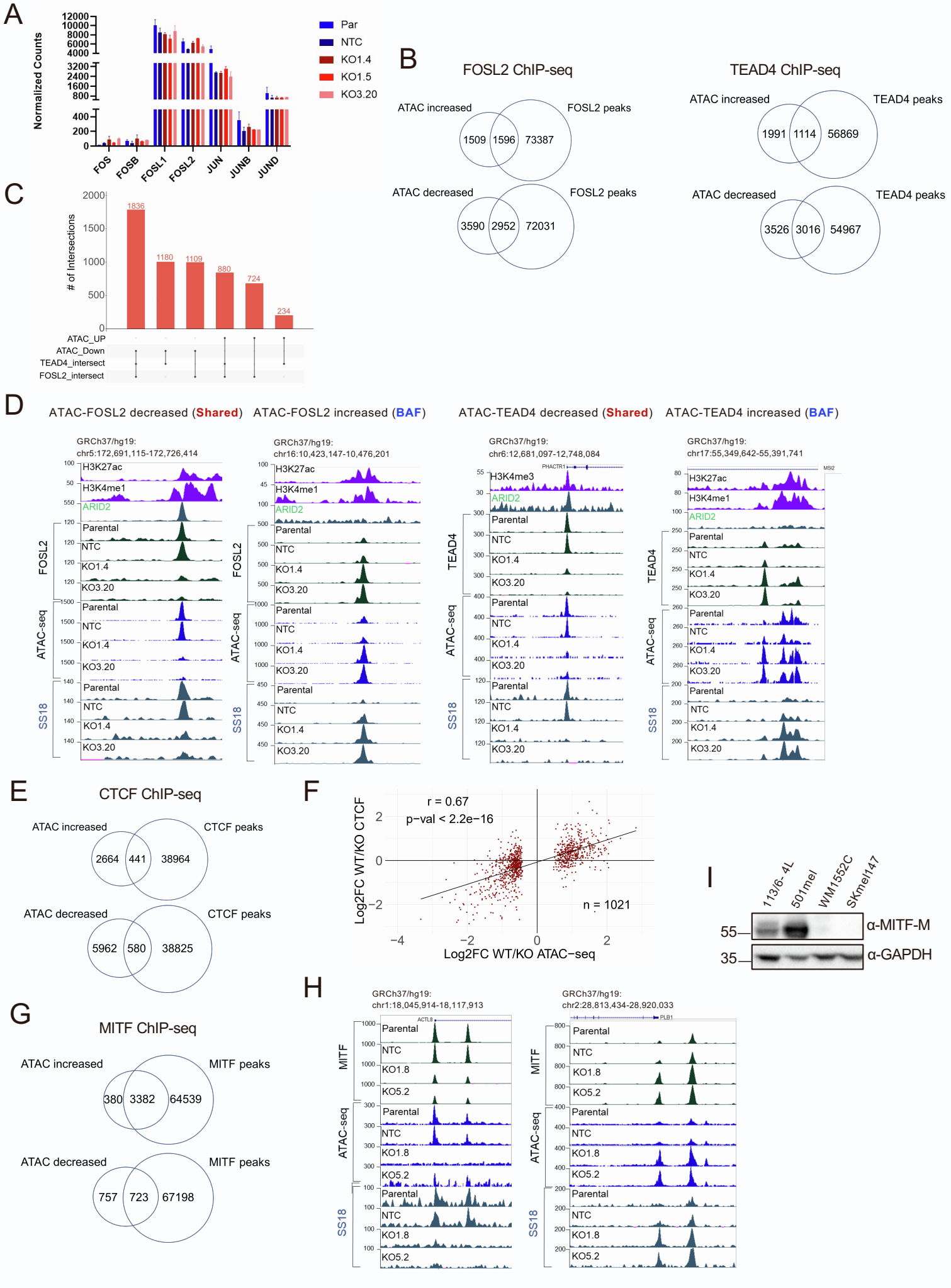
A
Normalized Counts
Par
NTC
KO1.4
KO1.5
KO3.20
FOS
FOSB
FOSL1
FOSL2
JUN
JUNB
JUND
B
FOSL2 ChIP-seq
ATAC increased
FOSL2 peaks
1509
1596
73387
ATAC decreased
FOSL2 peaks
3590
2952
72031
TEAD4 ChIP-seq
ATAC increased
TEAD4 peaks
1991
1114
56869
ATAC decreased
TEAD4 peaks
3526
3016
54967
C
# of Intersections
1836
1180
1109
880
724
234
ATAC_UP
ATAC_Down
TEAD4_intersect
FOSL2_intersect
D
ATAC-FOSL2 decreased (Shared)
ATAC-FOSL2 increased (BAF)
ATAC-TEAD4 decreased (Shared)
ATAC-TEAD4 increased (BAF)
GRCh37/hg19:
chr5:172,691,115-172,726,414
GRCh37/hg19:
chr16:10,423,147-10,476,201
GRCh37/hg19:
chr6:12,681,097-12,748,084
GRCh37/hg19:
chr17:55,349,642-55,391,741
H3K27ac
H3K4me1
H3K4me3
ARID2
Parental
NTC
KO1.4
KO3.20
FOSL2
TEAD4
ATAC-seq
SS18
E
CTCF ChIP-seq
ATAC increased
CTCF peaks
2664
441
38964
ATAC decreased
CTCF peaks
5962
580
38825
F
r = 0.67
p-val < 2.2e-16
n = 1021
Log2FC WT/KO CTCF
Log2FC WT/KO ATAC-seq
G
MITF ChIP-seq
ATAC increased
MITF peaks
380
3382
64539
ATAC decreased
MITF peaks
757
723
67198
H
GRCh37/hg19:
chr1:18,045,914-18,117,913
GRCh37/hg19:
chr2:28,813,434-28,920,033
MITF
ATAC-seq
SS18
Parental
NTC
KO1.8
KO5.2
I
113/6- 4L
501mel
WM1552C
SKmel147
55
35
α-MITF-M
α-GAPDH

Figure S4. PBAF and BAF changes alter distinct TF enrichment upon PBAF loss, Related to Figure 4. A. DEseq2 normalized counts (median of ratios) of AP-1 family TFs expressed in SKmel147 ARID2 WT and ARID2 KO clones. **B.** Intersection of ATAC increased and decreased regions with significantly called TEAD4 and FOSL2 peaks in SKmel147 ARID2 WT (Parental and NTC) and KO (KO1.4 and KO3.20) cells. **C.** Upset plot of the intersections between FOSL2, TEAD4 and ATAC deregulated peaks. **D.** Snapshots of the UCSC genome browser (GRCh37/hg19) showing FOSL2 and TEAD4 binding at ATAC decreased and increased regions, respectively. **E.** Intersection of ATAC increased and decreased regions with significantly called CTCF peaks in SKmel147 ARID2 WT (Parental and NTC) and KO (KO1.4 and KO3.20) cells. **F.** Scatterplot of SKmel147 ARID2 WT/KO log2 fold changes of CTCF with ATAC log2 fold changes at ATAC significantly increased and decreased regions. Pearson correlation displayed. **G.** Intersection of ATAC increased and decreased regions with significantly called MITF peaks in 501mel ARID2 WT (Parental and NTC) and KO (KO1.8 and KO5.2) cells. **H.** Snapshots of the UCSC genome browser (GRCh37/hg19) showing MITF binding at ATAC decreased and increased regions, respectively. **I.** Whole cell extract immunoblots of 4L, 501mel, WM1552C (primary melanoma), and SKmel147 cell lines probed for MITF (M isoform) and GAPDH as loading control.

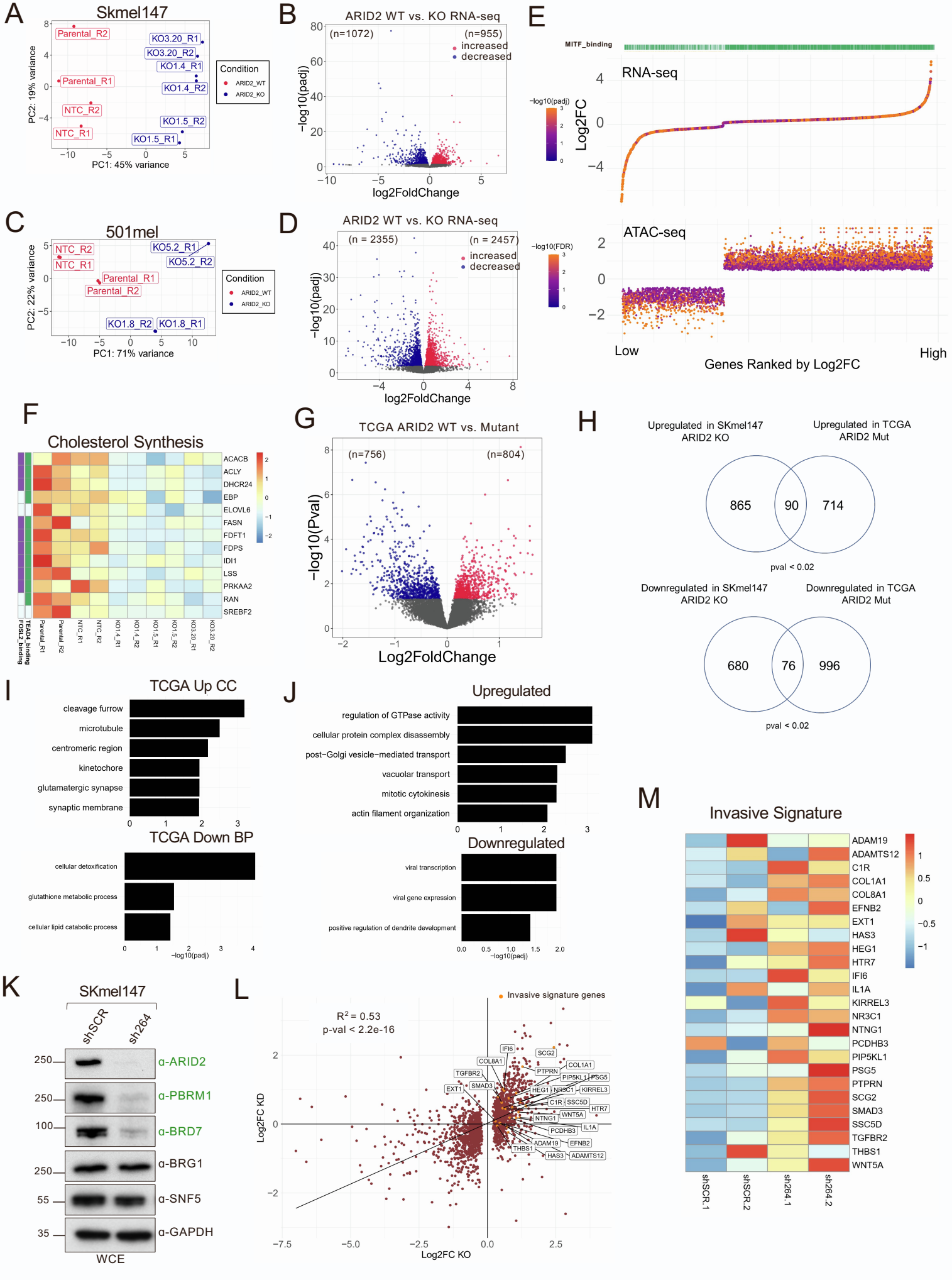
A
Skmel147
Parental_R2
KO3.20_R1
KO3.20_R2
KO1.4_R1
Parental_R1
KO1.4_R2
NTC_R2
KO1.5_R2
NTC_R1
KO1.5_R1
PC2: 19% variance
PC1: 45% variance
Condition
ARID2_WT
ARID2_KO
B
ARID2 WT vs. KO RNA-seq
(n=1072)
(n=955)
increased
decreased
−log10(padj)
log2FoldChange
C
501mel
NTC_R2
NTC_R1
KO5.2_R1
KO5.2_R2
Parental_R1
Parental_R2
KO1.8_R2
KO1.8_R1
PC2: 22% variance
PC1: 71% variance
D
ARID2 WT vs. KO RNA-seq
(n = 2355)
(n = 2457)
increased
decreased
−log10(FDR)
−log10(padj)
log2FoldChange
E
MITF_binding
RNA-seq
−log10(padj)
Log2FC
ATAC-seq
Low
High
Genes Ranked by Log2FC
F
Cholesterol Synthesis
ACACB
ACLY
DHCR24
EBP
ELOVL6
FASN
FDFT1
FDPS
IDI1
LSS
PRKAA2
RAN
SREBF2
TEAD4_binding
FOSL2_binding
Parental_R1
Parental_R2
NTC_R1
NTC_R2
KO1.4_R1
KO1.4_R2
KO1.5_R1
KO1.5_R2
KO3.20_R1
KO3.20_R2
G
TCGA ARID2 WT vs. Mutant
(n=756)
(n=804)
−log10(Pval)
Log2FoldChange
H
Upregulated in SKmel147 ARID2 KO
Upregulated in TCGA ARID2 Mut
865
90
714
pval < 0.02
Downregulated in SKmel147 ARID2 KO
Downregulated in TCGA ARID2 Mut
680
76
996
pval < 0.02
I
TCGA Up CC
cleavage furrow
microtubule
centromeric region
kinetochore
glutamatergic synapse
synaptic membrane
TCGA Down BP
cellular detoxification
glutathione metabolic process
cellular lipid catabolic process
−log10(padj)
J
Upregulated
regulation of GTPase activity
cellular protein complex disassembly
post−Golgi vesicle−mediated transport
vacuolar transport
mitotic cytokinesis
actin filament organization
Downregulated
viral transcription
viral gene expression
positive regulation of dendrite development
−log10(padj)
K
SKmel147
shSCR
sh264
α-ARID2
α-PBRM1
α-BRD7
α-BRG1
α-SNF5
α-GAPDH
WCE
L
Invasive signature genes
R² = 0.53
p-val < 2.2e-16
Log2FC KD
Log2FC KO
IFI6
SCG2
COL8A1
COL1A1
PTPRN
TGFBR2
PIP5KL1
PSG5
EXT1
SMAD3
HEG1
NR3C1
KIRREL3
C1R
SSC5D
HTR7
NTNG1
WNT5A
PCDHB3
IL1A
ADAM19
EFNB2
THBS1
HAS3
ADAMTS12
M
Invasive Signature
ADAM19
ADAMTS12
C1R
COL1A1
COL8A1
EFNB2
EXT1
HAS3
HEG1
HTR7
IFI6
IL1A
KIRREL3
NR3C1
NTNG1
PCDHB3
PIP5KL1
PSG5
PTPRN
SCG2
SMAD3
SSC5D
TGFBR2
THBS1
WNT5A
shSCR.1
shSCR.2
sh264.1
sh264.2

Figure S5. PBAF loss results in transcriptional changes that correlate with TF binding deregulation, Related to Figure 5. A. Two-dimensional PCA of all expressed genes SKmel147 ARID2 WT (Parental and NTC) and KO (KO1.4, KO1.5, and KO3.20) (n=17092) cells. **B.** Volcano plot highlighting significantly upregulated (n = 955) and downregulated (n = 1072) genes in SKmel147 cells as in (A). Deregulated genes were called with DEseq2 with an adjusted p-values < 0.05. **C.** Two-dimensional PCA of all expressed genes in 501mel ARID2 WT (Parental and NTC) and KO (KO1.8 and KO5.2) cells (n = 14833). **D.** Volcano plot highlighting significantly upregulated (n=2457) and downregulated (n = 2355) genes in 501mel cells as in (C). Deregulated genes were called with DEseq2 with an adjusted p-value < 0.05. **E.** Association of ranked deregulated genes in 501mel ARID2 KO vs. ARID2 WT cell lines with their associated ATAC increased or decreased peaks (within a TAD and within ±500 kb of the TSS) and their MITF status. **F.** Heatmap of significantly downregulated genes associated with ATAC decreased regions involved in the regulation of cholesterol synthesis in SKmel147. **G.** Volcano plot highlighting upregulated (n = 804) and downregulated (n = 756) genes in ARID2 mutant vs. ARID2 WT TCGA samples (n = 334). P-val < 0.05. **H.** Venn diagrams of deregulated genes intersected between SKmel147 and TCGA melanoma samples. Overlap significance calculated with Fisher's exact test. **I.** Gene Ontology (GO) analysis of genes upregulated and downregulated in TCGA ARID2 mutant vs. ARID2 WT in the Cellular Compartment (CC) and the Biological Process (BP) gene sets. **J.** Biological Process Gene Ontology (GO) analysis of genes associated with chromatin changes upregulated and downregulated in 501mel ARID2 KO vs. ARID2 WT cell lines. **K.** Whole cell extract immunoblots of SKmel147 cell lines infected with shScramble (shSCR) control or shRNA targeting ARID2 (sh264) probed for ARID2, PBRM1, BRG1, SNF5, and GAPDH as loading control. **L.** Scatterplot of SKmel147 ARID2 WT/KO log2 fold changes of all expressed genes with SKmel147 shSCR/sh264 log2 fold change, with invasive signature genes (same as in **Figure 5D**) highlighted. Pearson correlation displayed. **M.** Heatmap of invasive signature genes (as in **Figure 5D**) in SKmel147 infected with shSCR control or sh264 targeting ARID2.

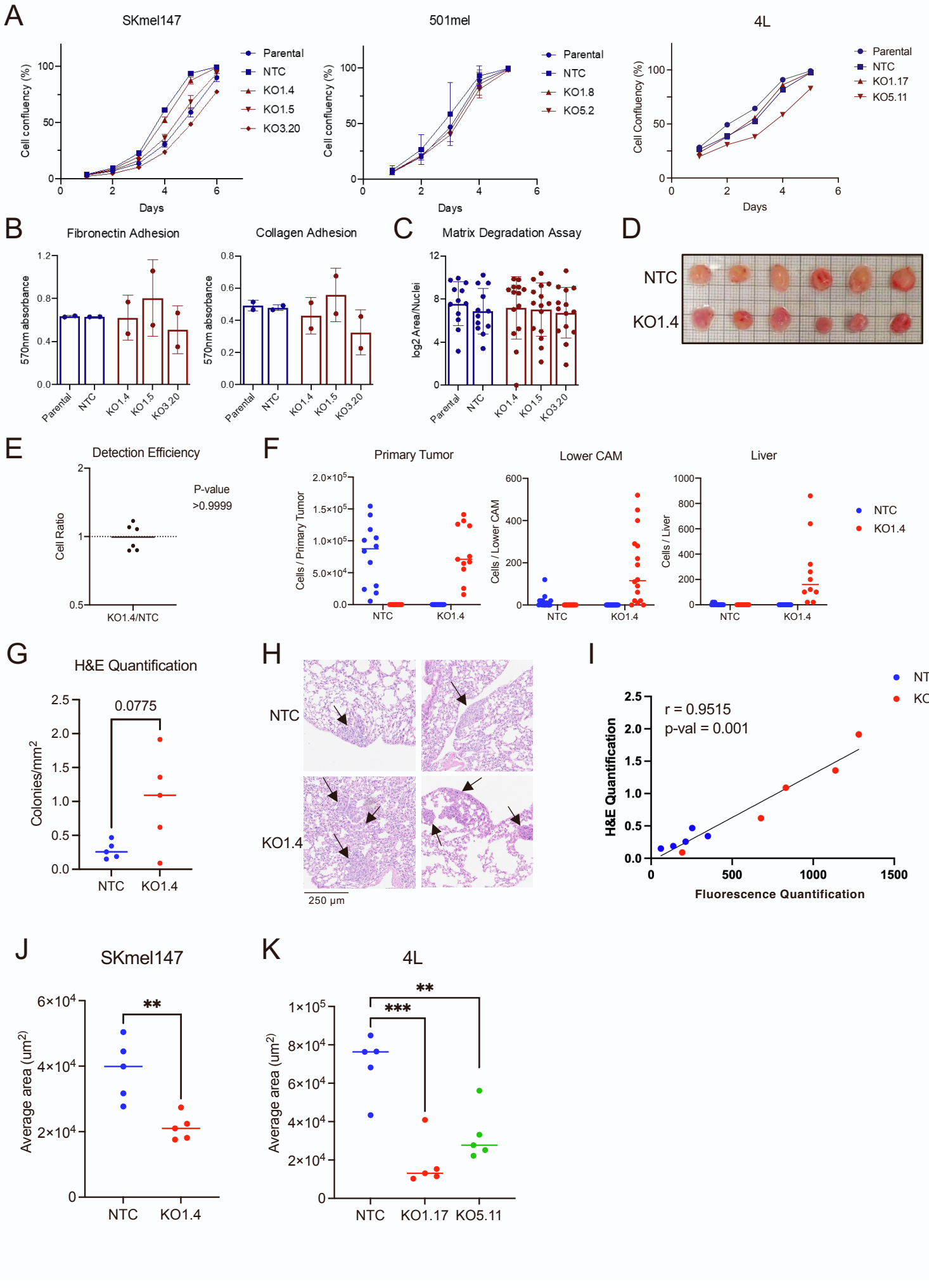
A
SKmel147
501mel
4L
Cell confluency (%)
Cell Confluency (%)
Days
Parental
NTC
KO1.4
KO1.5
KO3.20
KO1.8
KO5.2
KO1.17
KO5.11
B
Fibronectin Adhesion
Collagen Adhesion
570nm absorbance
C
Matrix Degradation Assay
log2 Area/Nuclei
D
NTC
KO1.4
E
Detection Efficiency
Cell Ratio
P-value
>0.9999
KO1.4/NTC
F
Primary Tumor
Lower CAM
Liver
Cells / Primary Tumor
Cells / Lower CAM
Cells / Liver
G
H&E Quantification
Colonies/mm2
0.0775
H
250 µm
I
r = 0.9515
p-val = 0.001
H&E Quantification
Fluorescence Quantification
J
SKmel147
Average area (um2)
**
K
4L
***

Figure S6. Assessing phenotypic changes upon PBAF loss in melanoma cells, Related to Figure 6. A. SKmel147 (n = 3), 501mel (n = 3), and 4L (n = 3) cell proliferation analysis measured over the course of 5-6 days as percent confluence. **B.** Adhesion assay of SKmel147 ARID2 WT and KO cells plated on fibronectin (n = 2) or collagen coated plates (n = 2). **C.** Matrix degradation assay of SKmel147 ARID2 WT and KO cells (n = 2). **D.** Image of primary tumors SKmel147 NTC (n=5) and KO1.4 (n = 5) collected from the CAM. **E.** Equal efficiency of Skmel147 ARID2 WT (GFP+) and KO (mCherry+) cell detection by flow cytometry, shown as the ratio of mCherry+ to GFP+ particles detected in samples spiked with equal numbers of WT and KO cells (non-inoculated CAM, n = 5; FACS buffer, n = 1). Y-axis is displayed on logarithmic scale. P-value shown for Wilcoxon signed-rank test for an expected median value of 1. **F.** Specificity of Skmel147 ARID2 WT (GFP+) and KO (mCherry+) cell detection by flow cytometry, shown as the complete absence of mCherry+ cells in eggs inoculated with WT cells, and of GFP+ cells in eggs inoculated with KO cells, in all samples analyzed in **Figure 6B**. **G.** Quantification of SKmel147 metastatic lung colonies from same mice as in **Figure 6D, E** based on H&E staining. Welch's t-test. P-value shown on graph. **H.** Representative H&E images of NTC and KO1.4 lung colonies same as in (G). **I.** Scatterplot of SKmel147 tail vein experiment quantification methods, either by fluorescence imaging in **Figure 6D, E** or H&E staining in (G). Spearman correlation is displayed. **J.** Quantification of the average area of SKmel147 metastatic lung colonies from mice in **Figure 6D, E**. Welch's t-test. **P-val < 0.01. **K.** Quantification of the average area of 4L metastatic lung colonies from mice in **Figure 6F**. Welch's t-test. **P-val < 0.01, ***P-val < 0.001.